

1 **Revision 1**

2 **A cotunnite-type new high-pressure phase of Fe₂S**

3 KENTA OKA¹, SHIGEHICO TATENO², YASUHIRO KUWAYAMA¹, KEI HIROSE^{1,2,*},
4 YOICHI NAKAJIMA³, KOIHIRO UMEMOTO², NORIYOSHI TSUJINO⁴, AND SAORI I.
5 KAWAGUCHI⁵

6
7 ¹Department of Earth and Planetary Science, The University of Tokyo, 7-3-1 Hongo, Bunkyo,
8 Tokyo 113-0033, Japan

9 ²Earth-Life Science Institute, Tokyo Institute of Technology, 2-12-1 Ookayama, Meguro, Tokyo
10 152-8550, Japan

11 ³Department of Physics, Kumamoto University, 2-39-1 Kurokami, Chuo, Kuammoto-shi,
12 Kumamoto 860-8555, Japan

13 ⁴Institute for Planetary Materials, Okayama University, 827 Yamada, Misasa, Tottori 682-0193,
14 Japan

15 ⁵Japan Synchrotron Radiation Research Institute, SPring-8, 1-1-1 Kouto, Sayo, Hyogo 679-5198,
16 Japan

17 * E-mail: kei@elsi.jp

18
19 **ABSTRACT**

20 We examined pressure-induced phase transitions in Fe₂S based on high-pressure and -
21 temperature X-ray diffraction measurements in a laser-heated diamond-anvil cell. Fe₂S is not stable
22 at ambient pressure but is known to form above 21 GPa with the Fe₂P-type (C22) structure. The

23 present experiments demonstrate a novel phase transition in Fe₂S from the C22 to C23 phase with
24 the Co₂P-type cotunnite structure above ~30 GPa. Our experiments also show the transformation
25 from the C23 to C37 (Co₂Si-type) phase above ~130 GPa. While these C23 and C37 structures
26 exhibit the same crystallographic symmetry (orthorhombic *Pnma*), the coordination number of
27 sulfur increases from nine in C23 to ten in C37. Such a sequence of pressure-induced phase
28 transitions in Fe₂S, C22 → C23 → C37, are similar to those of Fe₂P, while they are not known in
29 oxides and halogens that often adopt the C23 cotunnite-type structure. The newly found cotunnite-
30 type Fe₂S phase could be present in solid iron cores of planets including Mars.

31 **Keywords:** iron sulfide, high pressure, core, phase transition, cotunnite-type structure, Mars

32

33

INTRODUCTION

34 Sulfur is frequently observed in iron meteorites and could be a common impurity element in
35 planetary iron cores in our solar system and beyond. Solid iron sulfide can be an important
36 constituent in such metallic cores, although it is not dense enough for the Earth's inner core. Phase
37 relations in Fe-S alloy are of great importance to understand metallic cores of terrestrial planets.
38 While Fe-FeS is a simple binary eutectic system at ambient pressure, intermediate compounds of
39 Fe₃S, Fe₂S, and Fe₃S₂ form above 14–21 GPa (Fei et al. 2000). The phase relations and elastic
40 property of Fe₃S have been relatively well studied (e.g. Kamada et al. 2014; Thompson et al. 2020);
41 it does not undergo a structural phase change but decomposes into Fe + Fe₂S above ~250 GPa
42 (Ozawa et al. 2013; Mori et al. 2017; Bazhanova et al. 2017). In contrast, those of Fe₂S and Fe₃S₂
43 have been little investigated so far (Tateno et al. 2019).

44 It is known that Fe₂S adopts hexagonal *P-62m* Fe₂P-type (C22) structure at 22 GPa (Koch-
45 Müller et al. 2002). The recent experiments performed by Tateno et al. (2019) observed
46 orthorhombic *Pnma* Co₂Si-type (C37) structure in a pressure range from ~190 to 306 GPa. Phase
47 relations in Fe₂S remains unexplored by experiments between 22 and ~190 GPa, while theoretical
48 calculations showed that C37 Fe₂S is stable between 50 and 400 GPa (Bazhanova et al. 2017).
49 Tateno et al. (2019) reported the equation of state (EoS) of C37-type Fe₂S on the basis of
50 experimental data collected at 180 to 294 GPa, demonstrating that it is elastically anisotropic with
51 *a*-axis three times more compressible than *b*- and *c*-axes.

52 Iron sulfides are known to have affinities with iron phosphides (Stewart and Schmidt 2007; Gu
53 et al. 2014). A sequence of structural phase transitions have been already examined in Fe₂P;
54 hexagonal C22-type Fe₂P undergoes transformation to the orthorhombic Co₂P-type (cotunnite-
55 structured, C23) phase above 8 GPa and further to the Co₂Si-type (C37) phase above 42 GPa
56 (Nakajima et al. 2020). C23 and C37 Fe₂P are orthorhombic with the identical crystallographic
57 symmetry (space group: *Pnma*) but differ in the coordination number of phosphorus, leading to 2%
58 volume change across the phase transition. Similar isosymmetric phase transition is known in PbF₂
59 that occurs at ~10 GPa (Haines et al. 1998).

60 In order to reveal a sequence of phase transitions in Fe₂S, we carried out synchrotron X-ray
61 diffraction (XRD) measurements in-situ at high-pressure and -temperature (*P-T*) to 164 GPa and
62 2400 K in this study. The results demonstrate a stability of cotunnite-type (C23) Fe₂S between ~30
63 and ~130 GPa at high temperatures, indicating the sequence of pressure-induced structural phase
64 transitions (C22 → C23 → C37) which is similar to those in Fe₂P. The EoS of the new C23-type

65 Fe₂S phase is also reported. We discuss the possible presence of cotunnite-type Fe₂S in solid
66 metallic iron cores of planets including Mars and Mercury.

67

68

METHODS

69 XRD measurements were performed at high *P-T* in a laser-heated diamond-anvil cell (DAC)
70 at beamline BL10XU, SPring-8 (Hirao et al. 2020). We used diamond anvils with flat 300 μm or
71 beveled 120 μm culet size. Two different Fe₂S samples were used for starting materials; they were
72 synthesized by melting a mixture of Fe and FeS powder at 28 GPa and ~22 GPa in a multi-anvil
73 apparatus. The former is the same as that previously used in Tateno et al. (2019) and was employed
74 in runs #1–4. It consisted of a mixture of bcc Fe and FeS according to micro-focus X-ray
75 diffractometer measurements using a Cu *Kα* radiation source with 30 and 100 μm collimators.
76 Such observation is similar but different from that reported by Koch-Müller et al. (2002); they
77 observed that a majority of Fe₂S grains decomposed into Fe₃S + FeS when observed under a
78 transmission electron microscope.

79 In the first four runs, the sample assembly was MgO/SiO₂/Fe₂S/SiO₂, in which MgO was not
80 in contact with Fe₂S in order to avoid possible chemical reaction at high temperature. After loading,
81 a whole DAC was dried in a vacuum oven at 423 K for at least 1 hr to eliminate moisture in a
82 sample chamber, and then the sample was squeezed in an argon atmosphere. In run #5, Al₂O₃ was
83 used as a pressure medium and a pressure marker. After compression to a target pressure at room
84 temperature, we performed heating from both sides with single-mode fiber lasers. Heating spot size
85 was ~20 μm. Sample temperature was measured by a spectro-radiometric method. Pressure was
86 determined at 300 K from the volume of MgO (Wu et al. 2008) or Al₂O₃ (Dewaele and Torrent

87 2013). We corrected for thermal pressure of 5% pressure increase for each temperature increase of
88 1000 K following previous DAC experiments on silicate (Fiquet et al. 2010) and metals (Mori et
89 al. 2017). Such thermal pressure correction has been shown to be consistent with that considering
90 nearly isochoric heating in the Fe-C-H (Hirose et al. 2019) and Fe-FeO systems (Oka et al. 2019).
91 The overall pressure uncertainty was $\pm 5\%$ (Mori et al. 2017). Angle-dispersive XRD patterns were
92 collected on a flat panel detector (PerkinElmer XRD0822) (runs #1–4) and a CCD detector (Bruker
93 APEX) (run #5) (Fig. 1). A monochromatic X-ray beam energy was ~ 30 keV, and the incident X-
94 ray beam size was ~ 6 μm in full-width at half maximum. The variations in temperature within such
95 6 μm area at the hot spot were less than $\pm 10\%$. Collected XRD patterns were analyzed using the
96 IPAnalyzer and PDIndexer programs (Seto et al. 2010).

97 We additionally performed first principles calculations by adopting the Perdew-Burke-
98 Ernzerhof (PBE) form of generalized-gradient approximation (GGA) for the exchange-correlation
99 functional (Perdew et al. 1996). We used Vanderbilt-type pseudopotentials (Vanderbilt 1990). The
100 valence electron configurations and cutoff radii for pseudopotential generations are
101 $3s^2 3p^6 3d^{6.5} 4s^1 4p^0$ and 1.8 a.u. for Fe and $3s^2 3p^4$ and 1.7 a.u. for S (1 a.u. = 0.529177 Å). The cutoff
102 energy for the planewave expansion is 40 Ry, and the \mathbf{k} -point mesh was $4 \times 8 \times 4$. A smearing
103 technique (Methfessel and Paxton 1989) was used for integration up to the Fermi surface with a
104 smearing parameter of 0.005 Ry. We used the variable-cell-shape damped molecular dynamics for
105 structural optimization. The simulations were made for a unit cell including 12 (8Fe + 4S) atoms
106 ($Z = 4$). Dynamical matrices were calculated on the $2 \times 2 \times 2$ \mathbf{q} -point mesh using density-functional
107 perturbation theory (Giannozzi et al. 1991; Baroni et al. 2001). The vibrational contribution was

108 taken into account within the quasi-harmonic approximation (Wallace 1972). All calculations were
109 performed using the Quantum-ESPRESSO package (Giannozzi et al. 2009)

110

111

RESULTS

112 **New cotunnite-type Fe₂S phase**

113 We examined the phase relations in Fe₂S in four separate sets of high *P-T* experiments between
114 37 and 166 GPa (Fig. 2). In run #1, weak diffraction signal was observed from the sample when it
115 was compressed to 56 GPa at room temperature (Fig. 1a). When it was heated to 1800 K, we
116 observed new peaks in less than 3 min, all of which are assigned to the orthorhombic C23 structure
117 that has not been reported in Fe₂S (Figs. 1b, c). Similarly, the formation and the stability of the new
118 C23 Fe₂S phase were confirmed up to 115 GPa and 2300 K in run #2. In run #5, three different
119 spots in a sample were heated with increasing load pressure. The C23 phase was formed at
120 pressures as low as 37 GPa and 1650 K (Fig. 2).

121 In run #3, on the other hand, we observed broad diffraction peaks from the sample, whose
122 structure could not be identified, before heating at 300 K and ~150 GPa (Fig. 1d). Upon heating to
123 1500 K at 159 GPa, the C37 phase appeared in 2 min. The diffraction peaks from C37 Fe₂S grew
124 with increasing temperature to 2000 K at 163 GPa and further to 2400 K at 166 GPa. The overall
125 XRD pattern was assigned with C37-type Fe₂S and MgO (Figs. 1e, f).

126 These observations indicate that Fe₂S undergoes phase transitions from the C22 (Fe₂P-type) to
127 C23 (Co₂P-, cotunnite-type) structure above ~30 GPa and further to the C37 (Co₂Si-type) structure
128 above ~130 GPa (Fig. 2).

129

130 **Equation of state for C23 Fe₂S**

131 These C23- and C37-type Fe₂S exhibited the identical crystal symmetry, but their atomic
132 arrangements and lattice parameters are distinct (Table 1) (Tateno et al. 2019). Sulfur atom is
133 coordinated to nine and ten iron atoms in the C23 and C37 structures, respectively (Rundqvist
134 1960). Upon the phase transformation from the C23 to C37 structure, the orthorhombic unit cell is
135 shortened along *a*-axis but elongated along *b*- and *c*-axes as previously observed in Fe₂P (Nakajima
136 et al. 2020).

137 Figure 3 shows the pressure-volume (*P-V*) data at 300 K for the new C23 Fe₂S phase. The
138 revised compression curve for C37 Fe₂S is also given (Tateno et al. 2019). The unit-cell volume
139 was experimentally collected between 25 and 106 GPa after heating (or thermal annealing at less
140 than 1400 K) at each pressure. When collecting the *P-V* data, temperature was not quenched but
141 gradually decreased to room temperature to avoid nonhydrostatic stress in the sample. We also
142 obtained $V_0 = 134.24 \text{ \AA}^3$ at 1 bar and 300 K by first principles calculations. Such *P-V* data were
143 fitted by the Birch-Murnaghan EoS, giving bulk modulus $K_0 = 219(4)$ GPa at zero pressure and its
144 pressure derivative $K_0' = 4.1(2)$. We also obtained the revised EoS parameters of the C37 Fe₂S
145 phase by including the present new data at 153 GPa; $K_0 = 223(6)$ GPa with $K' = 4$ (fixed), and V_0
146 $= 133.4(8) \text{ \AA}^3$. The volume reduction upon C23 to C37 transition is calculated to be 0.8% at a
147 transition pressure of 130 GPa from their EoSs (Fig. 3). Since the transition occurs in Fe₂S at much
148 higher pressure, the volume change is smaller than those at similar isosymmetric phase transitions
149 in Fe₂P and PbF₂ which involve 2.3% and 2% volume reduction at 40 and 10 GPa, respectively
150 (Nakajima et al. 2020; Haines et al. 1998).

151

152

DISCUSSION

153 These results indicate that Fe₂S undergoes a series of structural phase transitions, C22 → C23
154 → C37, similar to Fe₂P (Dera et al. 2008; Nakajima et al. 2020). C23 is the AX₂ cotunnite-type
155 structure, widely observed in oxides and halogens. Nevertheless, the C22 to C23 and the C23 to
156 C37 transitions are hardly found in such oxides and halogens except for C22-type TiO₂ (note
157 however that C23 transforms into C22 with increasing pressure in TiO₂ according to Dekura et al.
158 2011) and C37-type PbF₂ (Haines et al. 1998), suggesting that they do not often form in ionic
159 materials. Alternatively, the C22 → C23 → C37 transitions may be common in M₂Y compounds
160 (M, 3d transition-metals such as Fe, Ni, and Co; Y, 3p-block elements such as Si, P, and S). Ni₂P
161 and Co₂P form in the C22 structure at 1 bar (Dera et al. 2009; Ellner and Mittemeijer 2001).
162 Theoretical calculations showed that C22 Ni₂P transforms into C23 at 77–88 GPa and 0–2000 K
163 (Inerbaev et al. 2020). C22 Co₂P changes into the C23 phase at low temperatures. Ni₂Si and Co₂Si
164 have the C37 structure at 1 bar (Errandonea et al. 2008; Geller and Wolontis 1955). The stability
165 of C37 Ni₂Si was confirmed experimentally to 75 GPa and theoretically to 400 GPa (Errandonea
166 et al. 2008).

167 These M₂Y phases exhibit coordination numbers (CN) of 4 and 5 for the M1 and M2 sites,
168 respectively, and 8 for Y for both the C22 and C23 phases. The volume difference between the two
169 structures are quite small (< 0.2%) (Ellner and Mittemeijer 2001; Dera et al. 2008). On the other
170 hand, while both the C22 and C23 phases of Co₂P and Fe₂P are ferromagnetic at ambient conditions,
171 the magnetic moments of C22 have been calculated to be much higher than those of C23 (Zhang
172 et al. 2011; Wu et al. 2010). The transition from the C22 to C23 structure in M₂Y including Fe₂S

173 could be caused by the decrease in magnetic moments of transition-metals and resulting volume
174 reduction.

175 The CN of Y in M_2Y increases from 9 to 10 upon C23 to C37 transition, which results in a
176 volume decrease much larger than that associated with C22 to C23 transition. As described above,
177 the C23 to C37 transition leads to 0.8% volume decrease in Fe_2S at 130 GPa (Fig. 3) and 2–2.3%
178 in Fe_2P and PbF_2 at 10–40 GPa (Nakajima et al. 2020; Haines et al. 1998). These C23 to C37 phase
179 changes could be also related to the depression of magnetic moments (or spin moments) of $3d$
180 transition-metals. It is supported by the facts that earlier calculations assuming the absence of spin
181 moments for Fe tend to overestimate the stability of C37 with respect to C23 in Fe_2P (Zhao et al.
182 2017) and Fe_2S (Bazhanova et al. 2017) when compared to experimental studies (Dera et al. 2008;
183 Nakajima et al. 2020).

184

185

IMPLICATIONS

186 The stability of cotunnite-type Fe_2S , first reported in the present experiments, ranges from ~30
187 to ~130 GPa, which overlaps with the pressure ranges of the cores of Mars (~20–45 GPa) and
188 Mercury (~7–40 GPa) (Tsujino et al. 2013 and references therein; Helffrich 2017) (Fig. 2). While
189 the Fe-FeS is a simple eutectic system at 1 bar, intermediate compounds of $Fe_{3+x}S_2$ (Fe + ~27 wt%
190 S, ≥ 14 GPa), Fe_2S (Fe + 22 wt% S, ≥ 21 GPa), and Fe_3S (Fe + 16 wt% S, ≥ 21 GPa) are formed
191 under high pressures (Fei et al. 1997, 2000; Koch-Müller et al. 2002). Fe_2S appears coexisting with
192 $Fe_{3+x}S_2$ or Fe_3S when 16 to ~27 wt% S is included in the Fe-S system at 21 GPa (Fei et al. 2000).

193 The SNC-meteorites that are believed to be derived from Mars are significantly depleted in all
194 chalcophile (sulfur-loving) elements, suggesting that the Martian core is enriched in sulfur much

195 more than the Earth's core that likely contains 1.7 wt% S from cosmo-/geochemical estimates
196 (Dreibus and Palme 1996). While a pioneer work by Dreibus and Wänke (1985) proposed 14.2
197 wt% S, more recent studies suggested higher sulfur concentrations (16–36 wt% S) (e.g. Zharkov
198 and Gudkova 2005; Khan and Connolly 2008; Rivoldini et al. 2011; Terasaki et al. 2018).
199 Constraining the chemical composition of the Mercury's core is more difficult, but the presence of
200 planetary magnetic field suggests that the core is molten at least partially, calling for the
201 incorporation of impurity element(s) such as sulfur that suppresses the melting temperature of iron
202 to a large extent (Fei et al. 2000; Stewart et al. 2007). Previous studies proposed the sulfur-rich
203 Mercury's core containing up to 36.5 wt% S (Harder and Schubert 2001; Chabot et al. 2014),
204 although the presence of silicon is also supported from reducing conditions at planetary surface.

205 Recent geodesy data, the moment of inertia and the Love number k_2 , indicate that at least the
206 outer part of the Mars' core is molten (Yoder et al. 2003; Rivoldini et al. 2011). Also, Mercury's
207 global magnetic field will require the liquid state of the core, and thermal evolution models suggest
208 the presence of a solid inner core (Dumberry and Rivoldini, 2015). Both Mars and Mercury may
209 thus have liquid outer core and solid inner core.

210 The detailed phase relations in the Fe-FeS system are known only to 21 GPa (Fei et al. 2000).
211 Fe₂S appears only in a narrow temperature range at this pressure, but the C22 to C23 phase
212 transition should expand the stability field of Fe₂S above ~30 GPa. Indeed, it may be supported by
213 the coexistence of Fe + Fe₂S (22 wt% S) rather than Fe + Fe₃S (16 wt% S) observed by Stewart et
214 al. (2007) at 40 GPa. It is also noted that Fe₂P exhibits a large liquidus field in the Fe-FeP system
215 even at 1 bar. The stability of Fe₂S was confirmed in the present study to 1650 K at 37 GPa in the
216 Martian core pressure range (Fig. 2). It agrees with the Mars' core temperatures that have been

217 recently estimated considering the presence of its inner core (Helffrich 2017). It is therefore
218 possible that C23 cotunnite-type Fe₂S is present in the solid inner core of Mars. It might appear in
219 the Mercurian core as well if Fe₂S is stable to higher temperatures or Mercury's core temperatures
220 are lower than currently estimated (Fig. 2).

221

222

ACKNOWLEDGMENTS AND FUNDING

223 XRD measurements were performed at the beamline BL10XU (proposals no. 2008B0099,
224 2018B0072, 2019A0072, and 2021A0072). First principles calculations were performed at Global
225 Scientific Information and Computing Center at the Tokyo Institute of Technology. This work was
226 supported by the JSPS grants no. 16H06285 and 21H04968 to K.H.

227

228

REFERENCES CITED

229 Baroni, S., de Gironcoli, S., Dal Corso, A., and Giannozzi, P. (2001) Phonons and related crystal
230 properties from density-functional perturbation theory. *Reviews of Modern Physics*, 73, 516–
231 558.

232 Bazhanova, Z.G., Roizen, V.V., and Oganov, A.R. (2017) High-pressure behavior of the Fe-S
233 system and composition of the Earth's inner core. *Uspekhi Fizicheskikh Nauk*, 187, 1105–1113.

234 Chabot, N., Wollack, E.A., Klima, R.L., and Minitti, M.E. (2014) Experimental constraints on
235 Mercury's core composition. *Earth and Planetary Science Letters*, 390, 199–208.

236 Dekura, H., Tsuchiya, T., Kuwayama, Y., and Tsuchiya, J. (2011) Theoretical and experimental
237 evidence for a new post-cotunnite phase of titanium dioxide with significant optical absorption.
238 *Physical Review Letters*, 107, 045701

- 239 Dera, P., Lavina, B., Borkowski, L.A., Prakapenka, V.B., Sutton, S.R., Rivers, M.L., Downs, R.T.,
240 Boctor, N.Z., and Prewitt, C.T. (2008) High-pressure polymorphism of Fe₂P and its implications
241 for meteorites and Earth's core. *Geophysical Research Letters*, 35, 1–6.
- 242 Dera, P., Lavina, B., Borkowski, L.A., Prakapenka, V.B., Sutton, S.R., Rivers, M.L., Downs, R.T.,
243 Boctor, N.Z., and Prewitt, C.T. (2009) Structure and behavior of the barringerite Ni end-member,
244 Ni₂P, at deep Earth conditions and implications for natural Fe-Ni phosphides in planetary cores.
245 *Journal of Geophysical Research*, 114, B03201.
- 246 Dewaele, A., and Torrent, M. (2013) Equation of state of α -Al₂O₃. *Physical Review B*, 88, 064107.
- 247 Dreibus, G., and Wänke, H. (1985) Mars, a volatile-rich planet. *Meteoritics*, 20, 367–381.
- 248 Dreibus, G., and Palme, H. (1996) Cosmochemical constraints on the sulfur content in the Earth's
249 core. *Geochimica Cosmochimica et Acta*, 60, 1125–1130.
- 250 Dumberry, M., and Rivoldini, A. (2015) Mercury's inner core size and core-crystallization regime.
251 *Icarus*, 248, 254–268.
- 252 Ellner, M., and Mittemeijer, E.J. (2001) The reconstructive phase transformation β -Co₂P \rightarrow α -
253 Co₂P and the structure of the high-temperature phosphide β -Co₂P. *Zeitschrift für anorganische*
254 *und allgemeine Chemie*, 627, 2257.
- 255 Errandonea, D., Santamaría-Perez, D., Vegas, A., Nuss, J., Jansen, M., Rodríguez-Hernandez, P.,
256 and Muñoz, A. (2008) Structural stability of Fe₅Si₃ and Ni₂Si studied by high-pressure x-ray
257 diffraction and ab initio total-energy calculations. *Physical Review B*, 77, 094113.
- 258 Fei, Y., Bertka, C.M., and Finger, L.W. (1997) High-pressure iron-sulfur compound, Fe₃S₂, and
259 melting relations in the system Fe-FeS at high pressure. *Science*, 275, 1621–1623.

- 260 Fei, Y., Li, J., Bertka, C.M., and Prewitt, C.T. (2000) Structure type and bulk modulus of Fe₃S, a
261 new iron-sulfur compound. *American Mineralogist*, 85, 1830–1833.
- 262 Fiquet, G., Auzende, A.L., Siebert, J., Corgne, A., Bureau, H., Ozawa, H., and Garbarino, G. (2010)
263 Melting of peridotite to 140 gigapascals. *Science*, 329, 1516–1518.
- 264 Geller, S., and Wolontis, V.M. (1955) The crystal structure of Co₂Si. *Acta Crystallographica*, 8,
265 83–87.
- 266 Giannozzi, P., Gironcoli, S., Pavone, P., and Baroni, S. (1990) *Ab initio* calculation of phonon
267 dispersions in semiconductors. *Physical Review B*, 43, 7231–7242.
- 268 Giannozzi, P., Baroni, S., Bonini, N., Calandra, M., Car, R., Cavazzoni, C., Ceresoli, D., Chiarotti,
269 G., Cococcioni, M., Dabo, I., and others (2009) QUANTUM ESPRESSO: a modular and open-
270 source software project for quantum simulations of materials. *Journal of Physics: Condensed*
271 *Matter*, 21, 395502.
- 272 Gu, T., Fei, Y., Wu, X., and Qin, S. (2014) High-pressure behavior of Fe₃P and the role of
273 phosphorus in planetary cores. *Earth and Planetary Science Letters*, 390, 296–303.
- 274 Haines, J., Léger, J.M., and Schulte, O. (1998) High-pressure isosymmetric phase transition in
275 orthorhombic lead fluoride. *Physical Review B*, 57, 7551–7555.
- 276 Harder, H., and Schubert, G. (2001) Sulfur in Mercury’s core? *Icarus*, 151, 118–122.
- 277 Helffrich, G. (2017) Mars core structure—concise review and anticipated insights from InSight.
278 *Progress in Earth and Planetary Science*, 4, 24.
- 279 Hirao, N., Kawaguchi, S.I., Hirose, K., Shimizu, K., Ohtani, E., and Ohishi, Y. (2020) New
280 developments in high-pressure X-ray diffraction beamline for diamond anvil cell at SPring-8.
281 *Matter and Radiation at Extremes*, 5, 018403.

- 282 Hirose, K., Tagawa, S., Kuwayama, Y., Sinmyo, R., Morard, G., Ohishi, Y., and Genda, H. (2019)
283 Hydrogen limits carbon in liquid iron. *Geophysical Research Letters*, 46, 5190–5197.
- 284 Inerbaev, T.M., Sagatov, N., Sagatova, D., Gavryushkin, P.N., Akilbekov, A.T., and Litasov, K.D.
285 (2020) Phase stability in nickel phosphides at high pressures. *ACS Earth and Space Chemistry*,
286 4, 1978–1984.
- 287 Kamada, S., Ohtani, E., Terasaki, H., Sakai, T., Takahashi, S., Hirao, N., and Ohishi, Y. (2014).
288 Equation of state of Fe₃S at room temperature up to 2 megabars. *Physics of the Earth and*
289 *Planetary Interiors*, 228, 106–113.
- 290 Khan, A., and Connolly, J.A.D. (2008) Constraining the composition and thermal state of Mars
291 from inversion of geophysical data. *Journal of Geophysical Research: Planets*, 113, E07003.
- 292 Koch-Müller, K., Fei, Y., Wirth, R., and Bertka, C.M. (2002) Characterization of high-pressure
293 iron-sulfur compounds. 33rd Lunar and Planetary Science Conference, Abstract #1424.
- 294 Methfessel, M., and Paxton, A. (1989) High-precision sampling for Brillouin-zone integration in
295 metals. *Physical Review B*, 40, 3616–3621.
- 296 Mori, Y., Ozawa, H., Hirose, K., Sinmyo, R., Tateno, S., Morard, G., and Ohishi, Y. (2017) Melting
297 experiments on Fe–Fe₃S system to 254 GPa. *Earth and Planetary Science Letters*, 464, 135–141.
- 298 Nakajima, Y., Araki, S., Kinoshita, D., Hirose, K., Tateno, S., Kawaguchi, S. I., and Hirao, N.
299 (2020) New pressure-induced phase transition to Co₂Si-type Fe₂P. *American Mineralogist*, 105,
300 1752–1755.
- 301 Oka, K., Hirose, K., Tagawa, S., Kidokoro, Y., Nakajima, Y., Kuwayama, Y., Morard, G.,
302 Coudurier, N., and Fiquet, G. (2019) Melting in the Fe-FeO system to 204 GPa: implications
303 for oxygen in Earth's core. *American Mineralogist*, 104, 1603–1607.

- 304 Ozawa, H., Hirose, K., Suzuki, T., Ohishi, Y., and Hirao, N. (2013) Decomposition of Fe₃S above
305 250 GPa. *Geophysical Research Letters*, 40, 4845–4849.
- 306 Perdew, J., Burke, K., and Ernzerhof, M. (1996) Generalized gradient approximation made simple.
307 *Physical Review Letters*, 78, 1396–1396.
- 308 Rivoldini, A., Van Hoolst, T., Verhoeven, O., Mocquet, A., and Dehant, V. (2011) Geodesy
309 constraints on the interior structure and composition of Mars. *Icarus*, 213, 451–472.
- 310 Rundqvist, S.T.I.G. (1960) The structures of Co₂P, Ru₂P and related phases. *Acta Chemica*
311 *Scandinavica*, 14, 1961–1979.
- 312 Seto, Y., Nishio-Hamane, D., Nagai, T., and Sata, N. (2010) Development of a software suite on
313 X-ray diffraction experiments. *The Review of High Pressure Science and Technology*, 20, 269–
314 276.
- 315 Stewart, A.J., and Schmidt, M.W. (2007) Sulfur and phosphorus in the Earth's core: the Fe-P-S
316 system at 23 GPa. *Geophysical Research Letters*, 34, L13201.
- 317 Stewart, A.J., Schmidt, M.W., van Westrenen, W., and Liebske, C. (2007) Mars: a new core-
318 crystallization regime. *Science*, 316, 1323–1325.
- 319 Tateno, S., Ozawa, H., Hirose, K., Suzuki, T., I-Kawaguchi, S., and Hirao, N. (2019) Fe₂S: the
320 most Fe-rich iron sulfide at the Earth's inner core pressures. *Geophysical Research Letters*, 46,
321 11944–11949.
- 322 Terasaki, H., Rivoldini, A., Shimoyama, Y., Nishida, K., Urakawa, S., Maki, M., Kurokawa, F.,
323 Takubo, Y., Shibasaki, Y., Sakamaki, T., and others (2019) Pressure and composition effects
324 on sound velocity and density of core-forming liquids: implication to core compositions of
325 terrestrial planets. *Journal of Geophysical Research: Planets*, 124, 2272–2293.

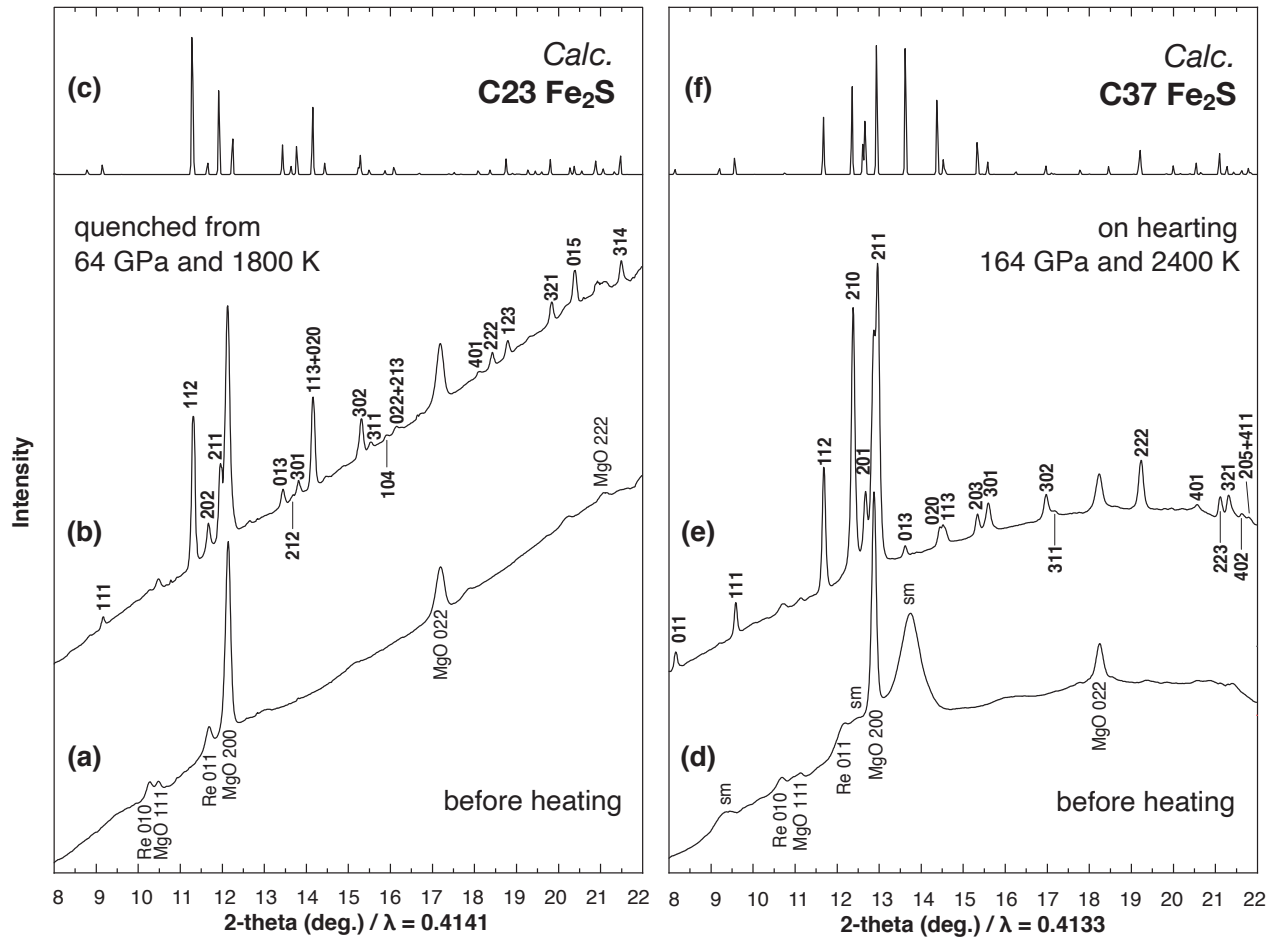
- 326 Thompson, S., Komabayashi, T., Breton, H., Suehiro, S., Glazyrin, K., Pakhomova, A., and Ohishi,
327 Y. (2020) Compression experiments to 126 GPa and 2500 K and thermal equation of state of
328 Fe₃S: implications for sulphur in the Earth's core. *Earth and Planetary Science Letters*, 534,
329 116080.
- 330 Tsujino, N., Nishihara, Y., Nakajima, Y., Takahashi, E., Funakoshi, K.-I., and Higo, Y. (2013)
331 Equation of state of γ -Fe: reference density for planetary cores. *Earth and Planetary Science*
332 *Letters*, 375, 244–253.
- 333 Vanderbilt, D. (1990) Soft self-consistent pseudopotentials in a generalized eigenvalue formalism.
334 *Physical Review B*, 41, 7892–7895.
- 335 Wallace, D.C. (1972) *Thermodynamics of Crystals*. Wiley.
- 336 Wu, X., and Qin, S. (2010) First-principles calculations of the structural stability of Fe₂P. *Journal*
337 *of Physics: Conference Series*, 215, 012110.
- 338 Wu, Z., Wentcovitch, R.M., Umemoto, K., Li, B., Hirose, K., and Zheng, J.D. (2008) Pressure-
339 volume-temperature relations in MgO: an ultrahigh pressure-temperature scale for planetary
340 sciences applications. *Journal of Geophysical Research*, 113, B06204.
- 341 Yoder, C.F., Konopliv, A.S., Yuan, D.N., Standish, E.M., and Folkner, W.M. (2003) Fluid core
342 size of Mars from detection of the solar tide. *Science* 300, 299–303.
- 343 Zhang, Q., Wu, X., and Qin, S. (2011) In situ high-pressure X-ray diffraction experiments and ab
344 initio calculations of Co₂P. *Chinese Physics B*, 20, 066101.
- 345 Zhao, Z., Liu, L., Zhang, S., Yu, T., Li, F., and Yang, G. (2017) Phase diagram, stability and
346 electronic properties of an Fe–P system under high pressure: a first principles study. *RSC*
347 *Advances*, 7, 15986–15991.

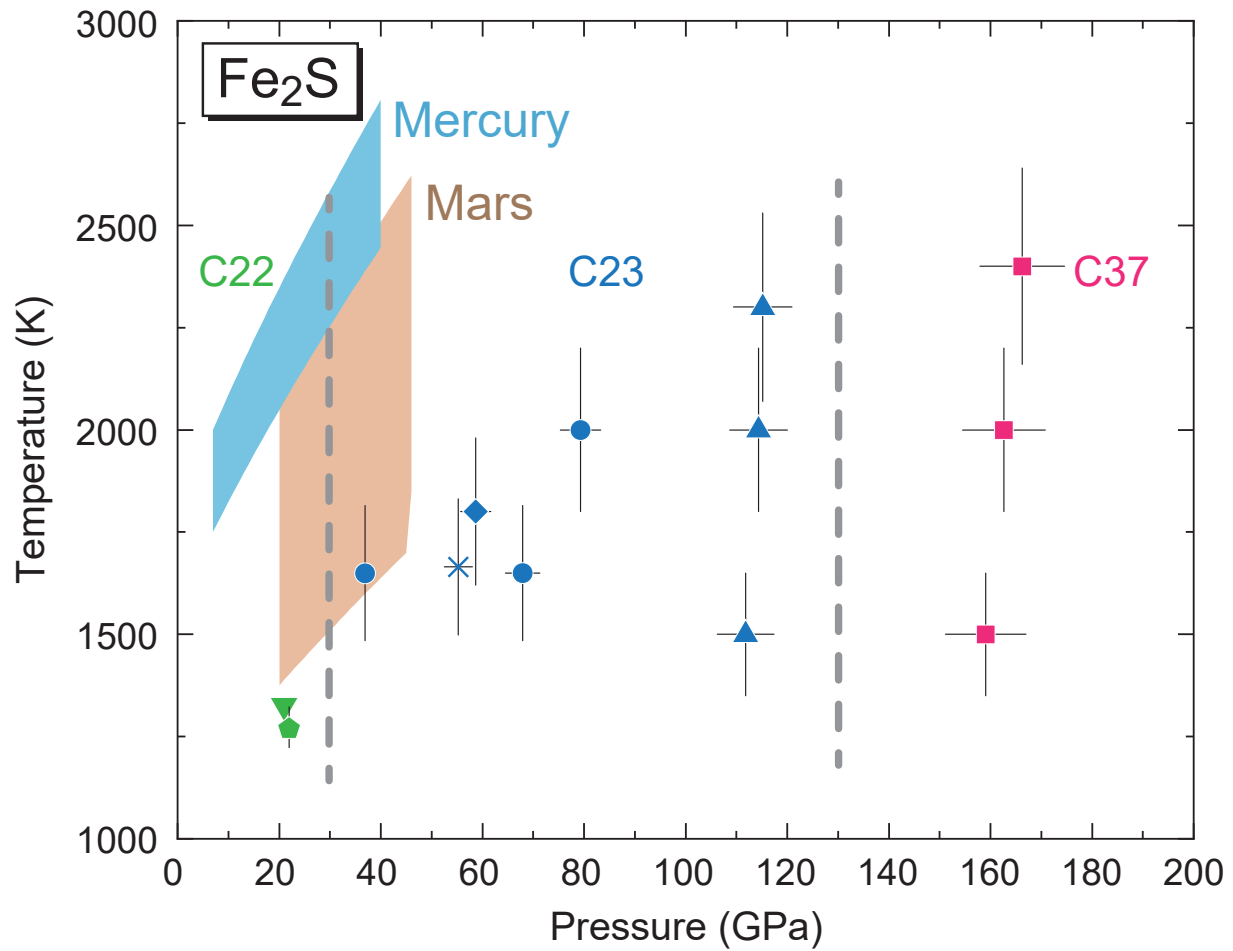
- 348 Zharkov, V.N., and Gudkova, T.V. (2005) Construction of Martian interior model. Solar System
349 Research, 39, 343–373.

350 **FIGURE 1.** XRD patterns in runs #1 (**a, b**) and #3 (**d, e**) collected at ~64 GPa and ~164 GPa,
351 showing the formations of the C23 cotunnite-type and C37 Fe₂S phases upon heating, respectively.
352 The calculated XRD patterns are given for the C23 (**c**) and C37 structures (**f**). sm; starting material.
353

354 **FIGURE 2.** Phase diagram of Fe₂S. The stabilities of the C22, C23, and C37 phases are shown by
355 green, blue, and red symbols, respectively. Reverse triangle, Fei et al. (2000); pentagon, Koch-
356 Müller et al. (2002); diamond, run #1; triangles, run #2; squares, run #3; cross, run #4; circles, run
357 #5. *P-T* conditions for the Martian (brown) and Mercurian cores (blue) are from Tsujino et al.
358 (2013) and Helffrich (2017).
359

360 **FIGURE 3.** Compression curves of C23 (blue) and C37 Fe₂S (magenta) at 300 K. Filled and open
361 symbols were data by experiments and calculations, respectively. Circles, data from this study
362 ([Table 1](#)); triangles, Tateno et al. (2019). See text for elastic parameters.





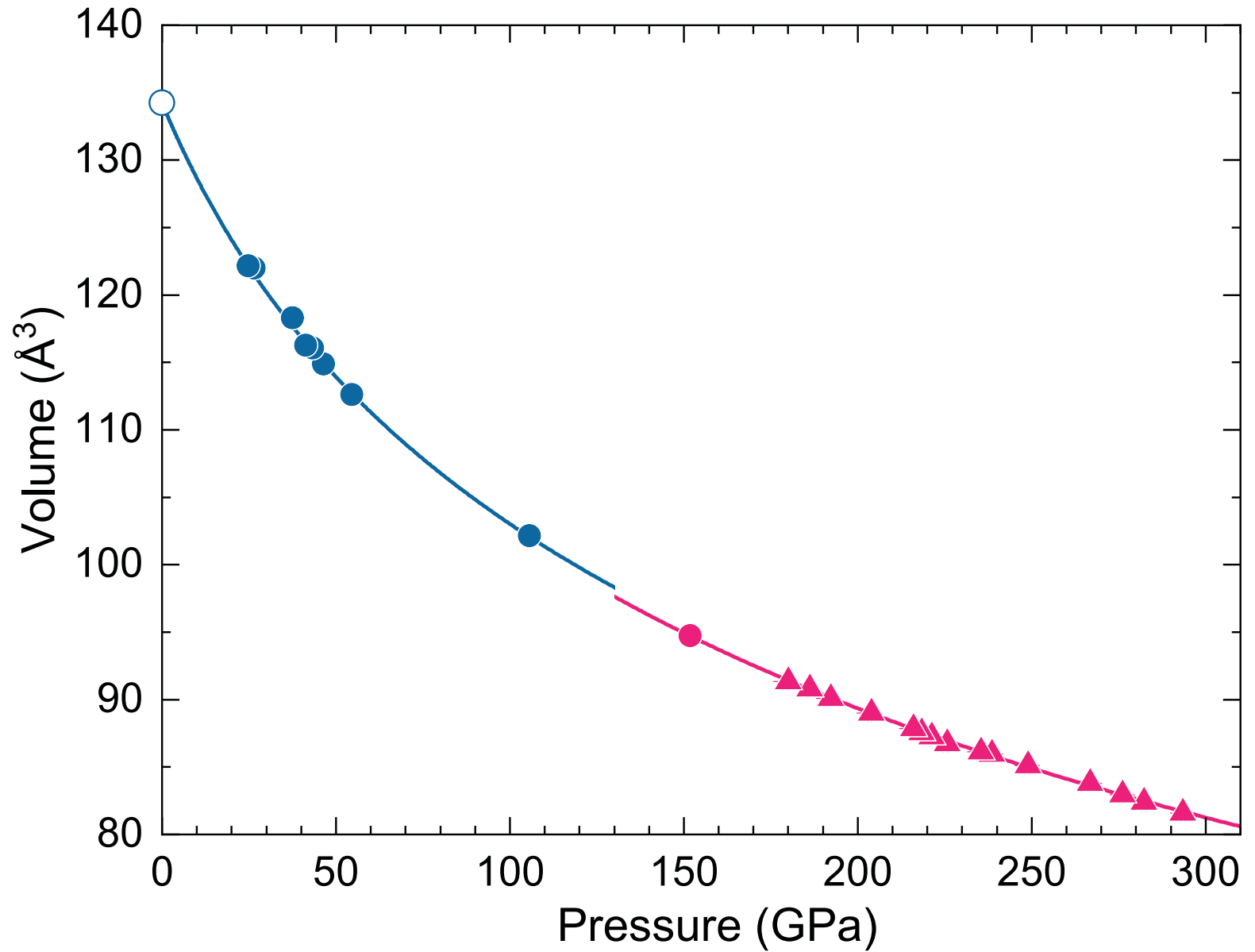


TABLE 1. Lattice parameters and volumes of C23- and C37-type Fe₂S at high pressure and 300 K

Structure	Pressure (GPa)	<i>a</i> (Å)	<i>b</i> (Å)	<i>c</i> (Å)	<i>V</i> (Å ³)
C23 ^a	0	5.863	3.586	6.384	134.24
C23	24.8(7)	5.572(6)	3.452(2)	6.352(5)	122.16(39)
C23	26.5(9)	5.563(8)	3.452(3)	6.353(6)	121.98(48)
C23	37.5(7)	5.497(6)	3.413(3)	6.304(6)	118.29(43)
C23	41.4(5)	5.458(2)	3.393(1)	6.278(2)	116.27(13)
C23	43.3(7)	5.451(1)	3.392(2)	6.276(2)	116.05(14)
C23	46.5(5)	5.427(1)	3.381(1)	6.261(2)	114.87(10)
C23	54.6(3)	5.380(3)	3.356(3)	6.236(6)	112.62(33)
C23	105.6(7)	5.054(3)	3.285(2)	6.149(6)	102.13(30)
C37	152.8(4)	4.679(3)	3.283(2)	6.165(5)	94.73(27)

^aTheoretically calculated at 0 GPa